A statistical-spectral method for echo classification

David A. Demer, George R. Cutter, Josiah S. Renfree, and John L. Butler

Demer, D. A., Cutter, G. R., Renfree, J. S., and Butler, J. L. 2009. A statistical-spectral method for echo classification. – ICES Journal of Marine Science, 66: 1081 – 1090.

The frequency dependence of sound-scatter intensity is commonly exploited to classify fish, zooplankton, and the seabed observed in acoustic surveys. Although less utilized, techniques based on the statistics of echo amplitudes can also be used to extract information. For example, single-frequency echo statistics have been used to determine whether backscatter originates from single or multiple fish or from rough or smooth seabeds, and to estimate scatterer sizes and densities. The efficacies of the amplitude-based techniques are challenged, however, by the usual requirement to group echo measurements to facilitate meaningful comparisons with model predictions. Groupings of data over space, time, or both, can combine scatter from multiple taxa or species, confounding the comparisons. These methods are improved with a hybrid, statistical-spectral method for target identification (SSID), which incorporates information contained in both the signal amplitudes and phases. The SSID uses multifrequency echo statistics from individual time-space intensities (pixels) to identify general scattering types, before applying model-based identification schemes for target identifications. The effectiveness of the SSID is demonstrated for fine-scale separation of scatter from demersal fish and the seabed and estimating seabed depth, within-beam slope, hardness and roughness, and the height of the dynamic acoustic dead zone.

Keywords: acoustic, classification, dead zone, demersal, EK60, hardness, ME70, multifrequency, rockfish, roughness, seabed, slope, split-beam, statistical, target.

Received 10 August 2008; accepted 10 January 2009; advance access publication 2 April 2009.

D. A. Demer, G. R. Cutter, J. S. Renfree and J. L. Butler: Southwest Fisheries Science Center, 8604 La Jolla Shores Drive, La Jolla, CA 92037, USA. Correspondence to D. A. Demer: tel: +1 858 546 5603; fax: +1 858 546 5656; e-mail: david.demer@noaa.gov.

Introduction

The distribution, abundance, and behaviour of marine organisms are commonly estimated with echo-integration methods, using calibrated echosounders operating at multiple frequencies. Successful application, however, requires attention to many details (Tesler, 1989; Demer, 2004). Foremost, it is imperative to apportion the backscattered amplitudes to each target type, filtering signals from unwanted scatterers co-existing in the survey area, and to estimate the distributions of backscattering cross sections (σ_{bs}) for each target type (Demer *et al.*, 1999). These steps are particularly challenging in areas with high species diversity and when fish are near the seabed. In addition, for studies of fish habitat and marine geology, accurate remote classification of the seabed is needed.

The frequency dependence of sound scatter is now commonly exploited for the remote identification of various scattering types (Greenlaw, 1979; Greenlaw and Johnson, 1983; Holliday *et al.*, 1989; Hewitt *et al.*, 2002). Other less utilized techniques involve scattering statistics to extract information on biotic and abiotic targets from their echoes (Clay and Heist, 1984; Stanton and Clay, 1986, and references to T. K. Stanton therein). For example, Trevorrow (1996) demonstrated that multifrequency measurements of volume-backscattering coefficients ($S_v = N_v\sigma_{bs}$) from calibrated, downward-looking echosounders can be combined with single-frequency echo statistics and simple scattering models to estimate σ_{bs} per animal and volume densities (N_v; animals m^{-3}). Here, it is established that those multifrequency and statistical methods, so classifications of animal and seabed types and estimates of σ_{bs} and N_v, can be improved through a hybrid, statistical-spectral method for acoustic target identification (SSID). The SSID uses multifrequency echo statistics to identify general scattering types, before averaging and applying model-based identification schemes for classifications. The SSID is particularly useful in studies of demersal fish.

Multifrequency target identification

Greenlaw (1979) demonstrated that differences in mean volume-backscattering strengths ($\overline{S_v} = 10\log(\overline{\sigma_{bs}}) + 10\log(\overline{N_v})$; dB re $1\ m^{-1}$) at two frequencies ($\Delta\overline{S_v}$) could be used to acoustically identify scatterer sizes. The overbar indicates an arithmetic mean taken in the linear domain. Holliday and Pieper (1980) and Greenlaw and Johnson (1983) found that additional frequencies could improve the accuracy of acoustically estimated zooplankton size distributions. In their method, scatterer sizes are remotely estimated by mathematically inverting one or more predictive models using multifrequency acoustic measurements of $\overline{S_v}$.

Korneliussen and Ona (2002) detailed techniques and software for automating such multifrequency target identifications. The techniques generally begin with a sequence of data preparations including noise removal, reductions of vertical and horizontal sampling resolutions, and data averaging. First, incoherent noise is computed and subtracted from the data at each frequency. The resulting noise-reduced S_v data are aligned vertically, compensating for the relative transducer positions, echo-pulse rise times and receiver delays. Then, importantly, the vertical and horizontal

sample resolutions are decreased through averaging to reduce natural stochastic fluctuations.

The efficacies of all of these multifrequency methods are challenged by the last step, which groups echo measurements to facilitate meaningful comparisons with model predictions. Groupings of data over space, time, or both can combine scatter from multiple taxa or species, or scatter from fish with that from the seabed, which can confound the comparisons.

Statistical target identification

Single-target echoes

Stanton and Clay (1986) explain that for a single scatterer that is resolvable in the insonified volume and has a small length (L) compared with the acoustic wavelength (λ; i.e. $L/\lambda \leq 1$), the echoes are weak and very similar, or coherent, within and between transmitted pulses. For larger scatterers (i.e. $L/\lambda \geq 15$), echoes from distributed anatomical features have different phases; they will interfere with each other and cause fluctuations (Demer and Conti, 2003), introducing some incoherence in the stronger returns.

Clay and Heist (1984) modelled σ_{bs} from single targets as the sum of concentrated or reflective components, the coherent signal (σ_{bs_c}), and the distributed or reverberant components, the random variation or incoherent noise (σ_{bs_d}). Likewise, the echo amplitude ($e = 10^{S_v/20}$) can be modelled as the sum of coherent (e_c) and incoherent (e_d) components:

$$e = e_c + e_d. \tag{1}$$

Similarly, Clay and Heist's (1984) ratio of coherent to incoherent echo intensities (γ) can be defined in terms of σ_{bs}, or e (proportional to $\sqrt{N_v \sigma_{bs}}$), yielding a metric for a type of signal-to-noise ratio (SNR):

$$\gamma = \frac{\sigma_{bs_c}}{\sigma_{bs_d}} = \frac{e_c^2}{e_d^2}. \tag{2}$$

The signal power is estimated by the coherent echo intensity (e_c^2), which is the square of the mean value of the random variable. The zero-mean noise power is equal to the variance of the random variable, which is estimated by the incoherent echo intensity (e_d^2). Following Clay and Heist (1984), Stanton and Clay (1986), and references to T. K. Stanton therein, the probability density function (PDF) of e is described by the two-parameter (mean and γ) Rician distribution (Figure 1a). When the echo amplitude is mostly coherent (i.e. concentrated, small, and/or stable target), γ becomes large and the Rician PDF approaches a Gaussian distribution, with $\bar{e} \approx \sqrt{\bar{\sigma}_{bs_c}}$ and sample variance

$$s^2(e) = \frac{1}{P-1} \sum_{p=1}^{P} (e_p - \bar{e})^2, \tag{3}$$

where p indices the P measurements made at one frequency. As γ increases, $s^2(e)$ tends to zero. Conversely, when the echo amplitude is mostly incoherent or noisy (i.e. large, distributed, and/or active target), γ approaches zero and the Rician PDF conforms to the Rayleigh distribution. For natural fish populations, γ ranges from near 0 to 12 (Dahl and Mathisen, 1983; Clay and Heist, 1984; Stanton and Clay, 1986).

Multiple-target echoes

For multiple, unresolved scatterers, the echoes further fluctuate because of interferences, increasing the incoherence and variance. Therefore, varying degrees of interference and incoherence occur when the echoes originate from the anatomical parts of an individual animal or from animals within an aggregation. The PDF of significantly overlapping echoes, at any instant, is Rayleigh. Moreover, the maximum e in a fixed time gate also has a Rayleigh PDF (Figure 1b) in the limit as the time gate becomes small compared with the ping duration (Stanton and Clay, 1986). As the time gate widens, assuming it includes more statistically independent measurements χ, the extremal PDF for overlapping echoes becomes Gaussian in shape (Figure 1c).

Interestingly, this theory indicates that as γ decreases, incoherence increases and the $\bar{e}$, which is generally assumed to be proportional to $\sqrt{N_v \sigma_{bs}}$ (Foote, 1983), decreases, potentially as much as 15% (Figure 1d) as the variance of e increases (Figure 1e). The SNR of the Rician PDF can be estimated by the dimensionless ratio of $\bar{e}$ and the standard error [$s(e)/\sqrt{P}$; Figure 1f]. Note that the variance of e increases as the ratio of coherent-to-incoherent echo amplitude decreases. Conversely, when the echo is dominated by coherent amplitudes, $s^2(e)$ and SNR tend to zero and infinity, respectively.

Another statistic, the variance-to-mean ratio in a time window (VMR; dB), can be used to characterize the dispersion or degree of randomness in a phenomenon (Figure 1g), and it too is modulated by γ. VMR can be modelled by the Poisson process, which at time t can be described by a Poisson PDF having equal variance and mean (VMR = 1.0). Spatial or temporal clustering corresponds to VMR > 1, whereas a more uniform, less random, distribution is indicated by VMR < 1.

Seabed echoes

This statistical theory is applicable to echoes from the seabed, as well as those from individual or aggregated animals (Stanton and Clay, 1986). Scatter originates from the many facets and features of the seabed, e.g. rocks, nodules, or ripples. The Rician PDF describes fluctuations of e for all ranges of seabed roughness: γ is large for flat and smooth seabeds, and small for those with moderate-to-high roughness. Echoes from smooth seabeds are characterized by a strong initial (reflected) component, and those from very rough seabeds are dominated by a later (scattered) component. Again, the variance of e depends on the level of incoherence, which is directly related to the seabed roughness.

Statistical-spectral identification

A combination of statistical and spectral techniques (SSID) may improve the accuracy of acoustic-target identification. The VMR can be used to preclassify each sample (pixel) within an echogram, allowing measurements from similar scatterers to be averaged for better comparison with model results. Moreover, the VMR can be used to estimate the coherence of echoes for the identification of individual (resolvable) targets and reflected and reverberant echoes from the seabed. Data from a survey of rockfish are used to explore these features.

Coast surveys

The Collaborative Optically Assisted Acoustic Survey Technique (COAST) was developed at the Southwest Fisheries Science Center to survey the dispersions and abundances of rockfish, by

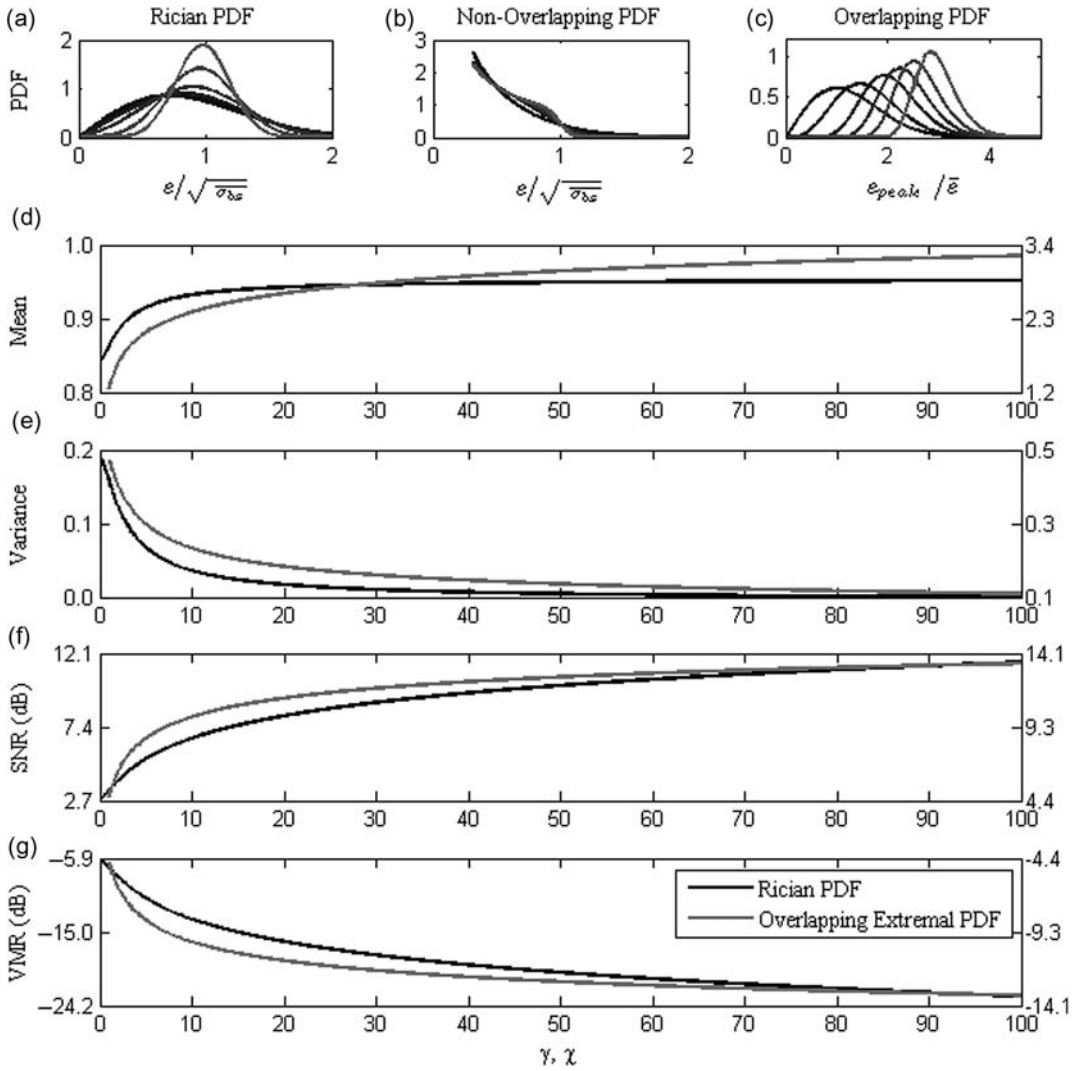

Figure 1. (a) Rician PDF, normalized by the mean (therefore, the integral over all e is 1.0), for $\gamma = 0.0$, 0.5, 1.0, 2.0, 5.0, and 10.0, dark to light lines, respectively. As γ increases from zero, the PDF transforms from a Rayleigh to a Gaussian PDF. (b) PDFs of extremal statistics for non-overlapping (resolvable) targets, with the number of independent samples per bin $\chi = 1$, 2, 5, 10, 20, and 50, dark to light lines, respectively. (c) PDFs of extremal statistics for overlapping (unresolvable) targets, with $\chi = 1$, 2, 5, 10, 20, and 50, dark to light lines, respectively; As χ increases, the distribution approaches a Gaussian shape. (d–g) Statistics of the Rician and overlapping extremal PDFs of normalized echo amplitudes vs. γ and χ, dark and light lines, respectively: (d) mean, (e) variance, (f) SNR, and (g) VMR, which is used to classify samples of sound scatter on fine (pixel) scales.

species, throughout the Southern California Bight (SCB). The technique uses historical fishing maps to define the survey sites initially, active-acoustics to map the dispersions and abundances of rockfish, and video and still images obtained with a remotely operated vehicle (ROV) to estimate the proportions and size-distributions of species in mixed assemblages. Rockfish in the SCB are generally associated with offshore banks, particularly in high-relief areas. This association makes it challenging to resolve the fish completely, even during daytime when they tend to rise above the seabed. The principal challenges of the acoustic surveys are to identify the echoes from rockfish accurately, resolve the acoustic scatter from those close to the highly reflective seabed, and estimate the unobserved volume near the seabed, the so-called acoustic dead zone (ADZ). The ADZ results from the finite dimensions of the acoustic beam and the seabed roughness.

Seabed depth and the ADZ

Acoustic measures of demersal and semi-demersal fish abundance may be underestimated because of: (i) dense aggregations of fish erroneously identified as seabed (MacLennan *et al.*, 2004), and (ii) the ADZ, where echoes from scatterers are combined with the seabed echo (Ona and Mitson, 1996). Techniques are available to account for the resulting biases (Ona and Mitson, 1996), but they assume a flat seabed and require accurate measurements of the vertical range to the seabed (MacLennan *et al.*, 2004).

When the acoustic wave front is nearly perpendicular to the seabed, the abrupt change in surface-backscattering strength ($\overline{S_s} = \overline{S_a}$; dB re 1 m^{-2}), which is equivalent to the area-backscattering strength (Manik *et al.*, 2006), can accurately indicate the instant when the beam axis intersects the seabed. Most fishery echosounders use this event to estimate automatically the seabed range. However, for the large incidence angles resulting

from steep or rough seabeds, the finite beam width causes early (negatively biased) detections of the seabed (MacLennan *et al.*, 2004).

Fortunately, in addition to the echo amplitude, split-beam echosounders provide two orthogonal, angular coordinates of the echo direction (Carlson and Jackson, 1980), commonly termed alongship (α; °) and athwartship (β; °). These angles are derived from the electrical-phase differences between transducer halves, using a conversion factor called the angle sensitivity ($\Lambda \approx kd_{\mathrm{eff}}$), where k is the acoustic wave number and d_{eff} the effective separation of the transducer halves (Demer *et al.*, 1999). More accurate seabed detection can be achieved if these angle measurements are used to correct the echo amplitude for the transducer directivity (Shirazi *et al.*, 1992).

The slope and roughness of the seabed within the beam footprint can be estimated from the split-beam angles and their variance, respectively. At larger angles of incidence, the split-beam angles are initially large when the edge of the beam intersects the shallowest seabed; they decrease for scatter near the beam-axis, then increase again, but in opposite polarity, as the beam intersects deeper seabed. The time at which the split-beam angles cross zero indicates when the beam axis intersects the seabed vertically. At this moment, the range to the seabed is the best estimate of the depth beneath the transducer, assuming that the pitch and roll of the transducer are taken into account.

Seabed classification

Sound scatter from the seabed depends on the acoustic wavelength (λ), the seabed reflectivity, roughness, and slope (θ), and the insonified area contributing to the instantaneous signal. The latter depends on the beam and seabed geometries and the detection range. Taking account of the equivalent two-way beam angle (ψ), θ, and the vertical range to the seabed (z), the multifrequency $\bar{S}_s$ from coherent seabed echoes can provide estimates of the seabed reflectivity, an indication of hardness, and the root-mean-square (rms) roughness (ρ). Additionally, the incoherent seabed echoes and the variance of the signal phase, both modulated by the degree of echo interference, can also provide estimates of the seabed roughness.

Methods

Coast surveys

Data from the 2005 COAST survey of the 43 Fathom Bank, located ~40 nautical miles west of San Diego, CA, were used to demonstrate the new SSID. The survey was conducted from the sportfishing vessel "Outer Limits" equipped with a five-frequency (18, 38, 70, 120, and 200 kHz) echosounder (Simrad EK60) and a hull-mounted transducer array. The transducers (Simrad ES18-11, ES38B, ES70-7C, ES120-7C, and ES200-7C) were spaced to maximize the overlap of insonified volumes and minimize the vertical offsets. The echosounders were calibrated before the surveys using a standard sphere (38.1 mm diameter, tungsten-carbide, with 6% cobalt binder).

As rockfish generally rise above the seabed during daytime, the surveys were conducted only between sunrise and sunset at a cruising speed of 7–10 knots. The track lines were 0.2 nautical miles apart. At each frequency, synchronized pulses with durations $\tau = 512$ μs were transmitted at intervals of 1 s and propagated at the sound speed $c \approx 1515$ m s^{-1}. Pulses with length $c\tau = 0.7757$ m with bandwidths of 1.749, 3.275, 4.687, 5.557, and 5.972 kHz, corresponding to the frequencies listed above, were received and sampled every 128 μs (four samples per pulse), providing samples of S_v every 0.097 m in range. S_v corresponding to ranges up to 500 m beneath the transducers were recorded continuously for each frequency.

Variance-to-mean ratio

The theory of echo-statistics described earlier can be extended to F measurements of echo amplitude, e, made concurrently from the same insonified volume at several discrete frequencies. The pth measurement at a given time and space (pixel) and the fth frequency ($\sigma_{\mathrm{bs}_{p,f}}$), along with their means and variances, depend on the scatterer morphology, shape, size, position in the beam, off-normal incidence angle (ϕ), and N_v. The resulting distribution is a combination of different PDFs for each frequency. For low N_v, these PDFs are each the convolution of the Rician PDF for a single target and the PDF caused by beam-pattern effects (Peterson *et al.*, 1976; Clay, 1983; Stanton and Clay, 1986). For overlapping echoes, these PDFs are each the convolution of interfering echoes and the PDF from beam-pattern effects. Therefore, the distributions differ to an extent depending on the transducer beam width, the spread of frequencies, the scattering spectra of the targets, and their size, roughness, and behaviour. With constant beam widths and frequencies, the distributions are modulated only by the scatterers.

For synchronized multifrequency echosounders with co-located transducers having similar beam widths, the $\sigma_{\mathrm{bs}_{p,f}}$ originate from the same scatterer(s) and are somewhat covariant. As previously discussed, however, measurements with different L/λ, N_v, and target behaviour will include different amounts of interference, modulating the measurement variances and means.

The VMR, used to characterize dispersion or degree of randomness in a phenomenon, is

$$\mathrm{VMR} = 10\log\left(\frac{1/(F-1)\sum_{f=1}^{F}(e_{p,f}-\overline{e_p})^2}{\overline{e_p}}\right), \text{where } \overline{e_p} = \frac{\sum_{f=1}^{F} e_{p,f}}{F}. \quad (4)$$

The VMR is also a useful metric for finely apportioning echoes to the various general types of scatterer present. Fundamentally, this is because the sample variance includes information about the ratio of coherent-to-incoherent echo amplitude. VMR has a larger dynamic range than SNR because the standard deviation, which is highly correlated with $\overline{\sigma_{\mathrm{bs}_p}}$, is squared in the numerator. VMR therefore includes combined information on the type, size, and number of volume scatterers, and surface hardness and roughness.

Target preclassification

Noise in the S_v at 18 and 38 kHz (Figure 2a) was generally negligible. Noise in the 70, 120, and 200 kHz data were removed as described in Hewitt *et al.* (2002). Next, the VMR values from the noise-reduced, five-frequency S_v data were rendered as an echogram (using the Formula operator in Echoview V4.40; Figure 2b). Empirical ranges of the VMR were used to identify the aggregations of fish with swimbladders (−40 to −23 dB; Figure 2d), the coherent reflection from the seabed (−23 to +5 dB; Figure 2c), and the incoherent reverberation from the seabed (−40 to −23 dB; Figure 2d). The VMR may be inversely related to sampling volume, the potential number of scatterers

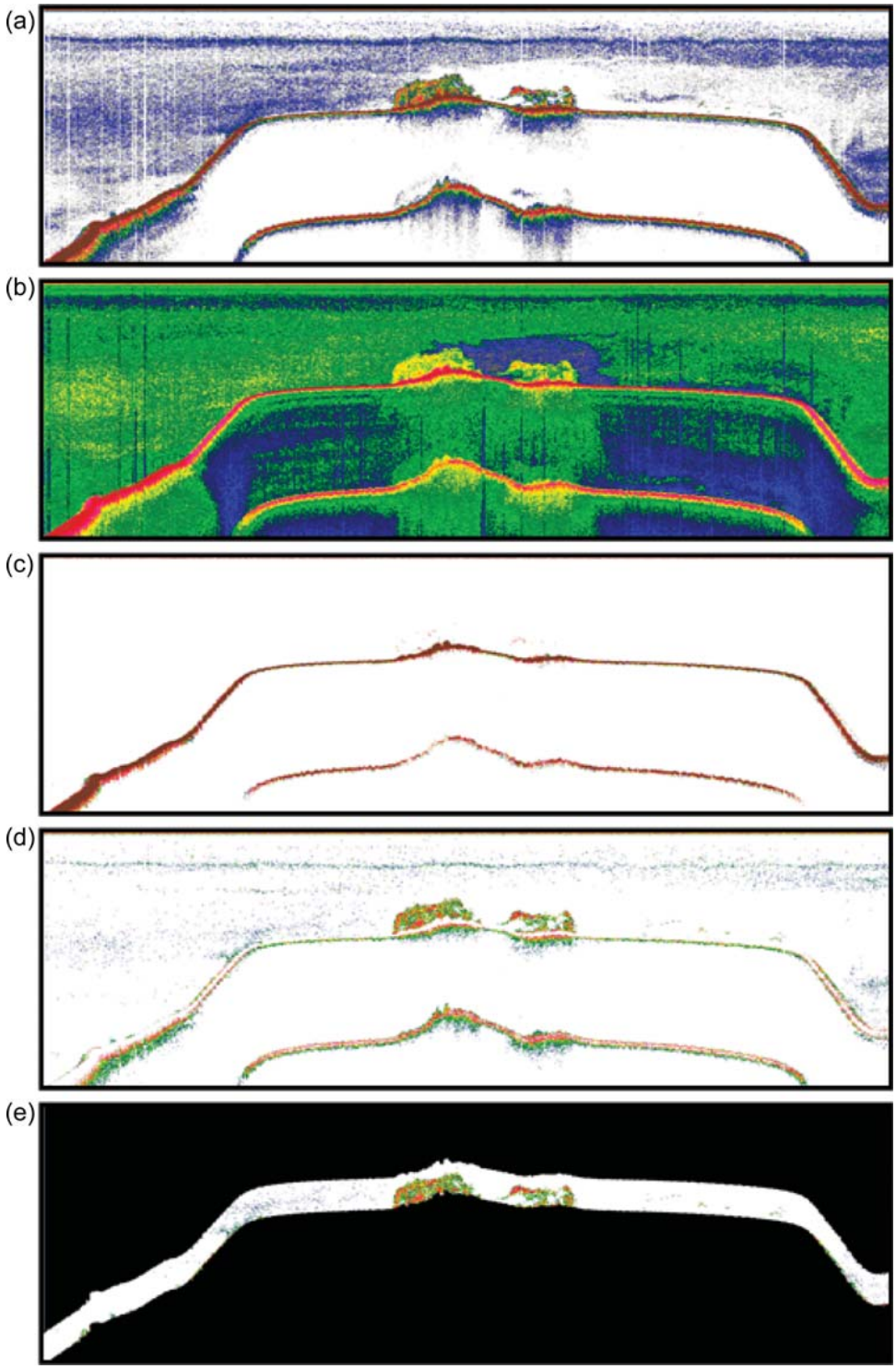

Figure 2. (a) A 38 kHz echogram illustrating aggregations over a high-relief rocky seabed; (b) VMR echogram providing high temporal-spatial resolution of the incoherent scatter from the aggregations of rockfish, the coherent initial reflection from the seabed, and the subsequent incoherent reflection, primarily from the rough seabed; (c) the coherent (reflected) echo from the seabed at 38 kHz; (d) the incoherent echoes from the aggregations of rockfish and the rough seabed; and (e) echoes at 38 kHz from the putative aggregations of rockfish.

contributing to the echo, and thus range. The fish with swimbladders within 40 m of the seabed were putatively identified as rockfish (Figure 2e).

Following this preclassification, but not demonstrated here, the S_v attributed to rockfish is integrated, resulting in nautical-area-scattering coefficients (s_A; m^2 nautical $mile^{-2}$). These are apportioned to the various species present, estimated using visual observations from the ROV, with proportions based on the σ_{bs} (L) weighted by the PDF of L, also estimated from visual observations, for each species. The area-densities N_a

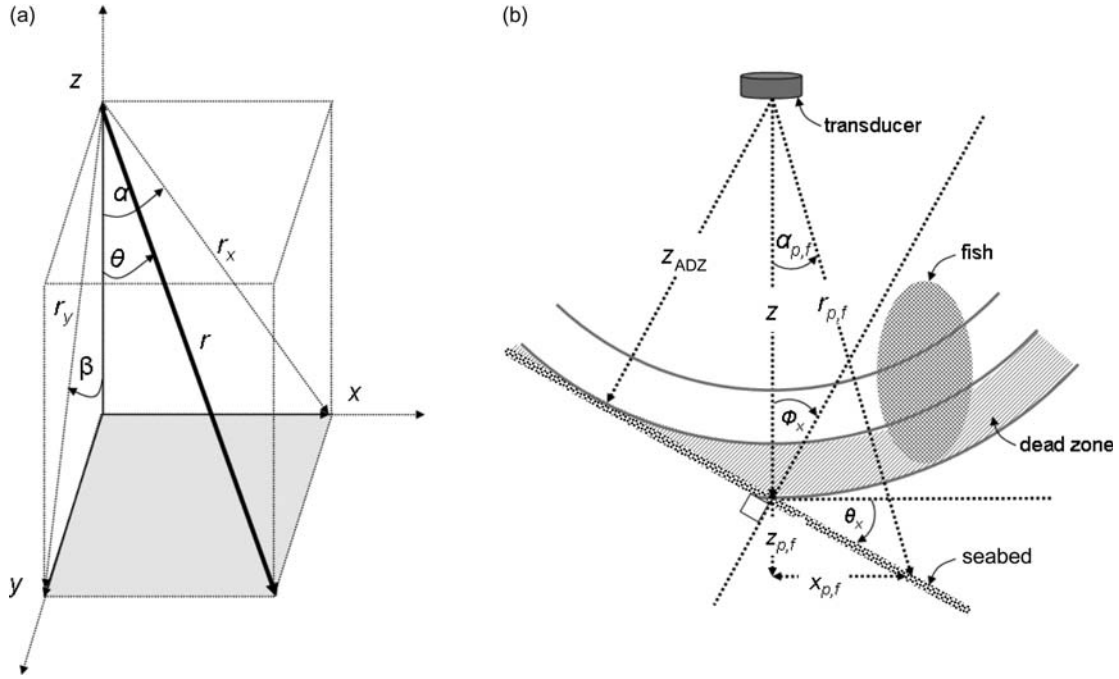

Figure 3. (a) Geometry of the split-beam angle measurements used for estimating local seabed slope; (b) The height of the ADZ estimated from the difference between the range of the initial coherent echo from the seabed (z_{ADZ}) and the range when the beam axis intersects the seabed (z). The echo-integrator dead zone (IDZ; see Ona and Mitson, 1996) is the sum of the ADZ, a backstep zone, and a partial-integration zone.

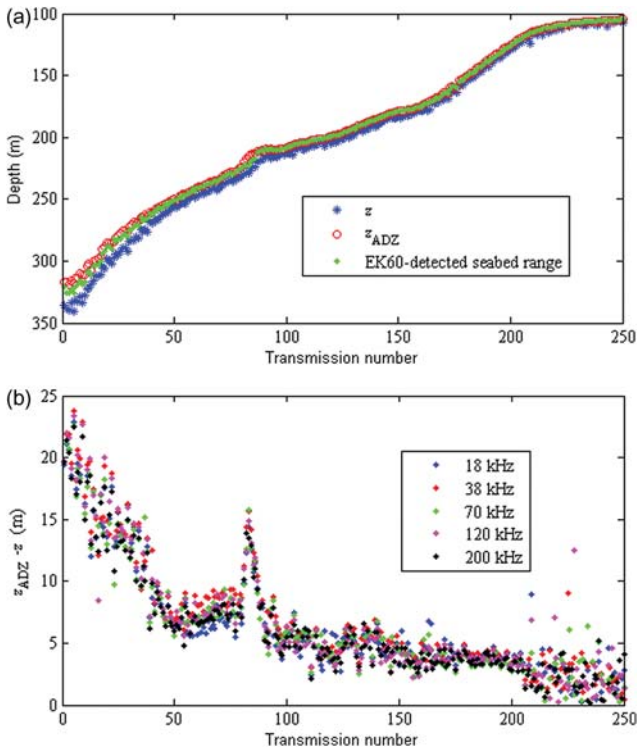

Figure 4. (a) The range of the initial coherent echo from the seabed (z_{ADZ}), the EK60-detected seabed range, and the range when the beam axis intersects the seabed (z), from 18 kHz data; and (b) the height of the dynamic ADZ ($h_{ADZ} = z - z_{ADZ}$) for each of 250 transmissions at five frequencies, progressing from deep water, up the bank, and onto the flat, but rocky plateau.

(fish m^{-2}) of each rockfish species are then estimated from the ratio of the mean s_A for each species divided by the length-weighted $\overline{\sigma_{bs}}$. To estimate the latter, models of TS vs. L and f are used.

Dead-zone estimation

As described in Ona and Mitson (1996), ψ, τ, and z contribute to the ADZ, as do θ, ρ, and transducer motion. With constant ψ and τ, and assuming negligible transducer motion, the height of the ADZ (h_{ADZ}) is modulated by the dynamic z, θ, and ρ. To estimate this component of measurement bias, the VMR is used to determine the earliest pixel from each transmission when relatively incoherent scatter from targets in the water cannot be resolved from the coherent seabed echo. This range (z_{ADZ}), defining the start of the ADZ, was estimated from the shortest range of the coherent seabed return (identified by VMR as being in the range −23 to +5 dB).

To estimate z and θ (Figure 3), P sets of $\alpha_{p,f}$, $\beta_{p,f}$, and $r_{p,f}$ measured within the coherent seabed echo were transformed to P sets of $x_{p,f}$, $y_{p,f}$, and $z_{p,f}$ following Conti *et al.* (2005):

$$\begin{bmatrix} x_{p,f} \\ y_{p,f} \\ z_{p,f} \end{bmatrix} = \frac{r_{p,f}}{\sqrt{1 - \sin^2 \alpha_{p,f} \sin^2 \beta_{p,f}}} \begin{bmatrix} \sin \alpha_{p,f} \cos \beta_{p,f} \\ \cos \alpha_{p,f} \sin \beta_{p,f} \\ \cos \alpha_{p,f} \cos \beta_{p,f} \end{bmatrix}. \quad (5)$$

For each transmission and frequency, these Cartesian distances were fitted with a plane ($z = a_f\, x + b_f\, y + z_f$), using the method of least-squares. The range where the beam-axis intersected the seabed (z_f) was estimated from this plane, with $x = y = 0$. The

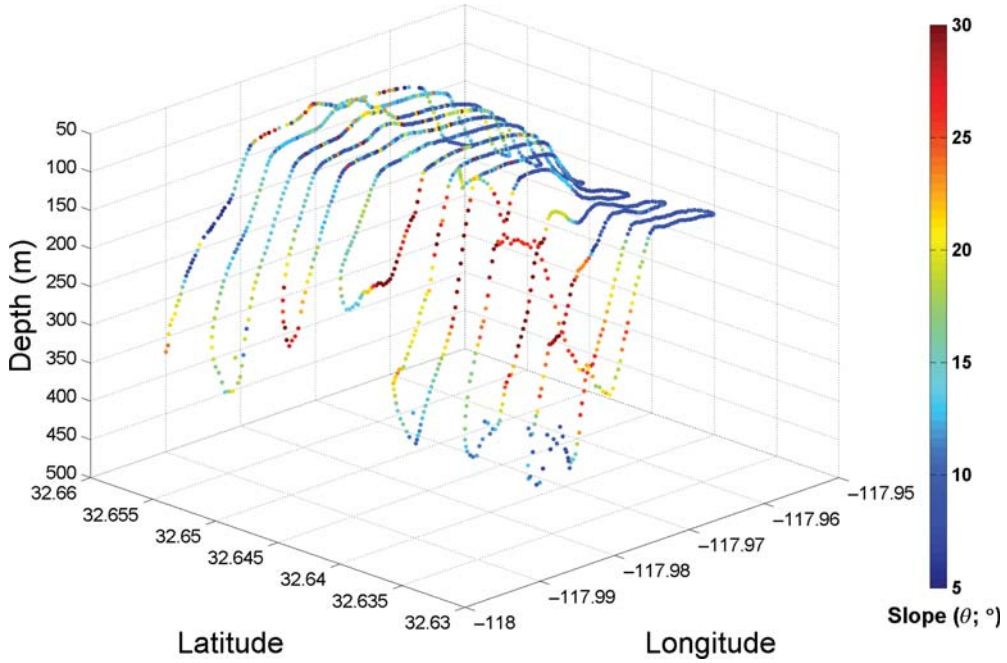

Figure 5. Local seabed slope plotted vs. latitude, longitude, and depth for 18 kHz. The measurements of local slope (θ_f) depend on the seabed roughness, transducer beam width and motion, and the accuracy of the angle sensitivity (Λ), which converts measurements of electrical phase to physical angles. Disregarding the sample-resolution mismatch, comparison of θ_f with slopes estimated from the multibeam bathymetry (Figure 6) indicate agreement to within 2° on the high-slope edges of the bank and low-slope sandy areas. As expected, however, θ_f is sensitive to fine-scale structure and is therefore much more variable in the high-relief rocky areas on the top of the bank.

h_{ADZ} were estimated for each transmission and frequency (Figure 4):

$$h_{\mathrm{ADZ}_f} = z_f - z_{\mathrm{ADZ}_f}. \tag{6}$$

The θ_f were also estimated from this plane using

$$\theta_f = \cos^{-1}\left(\frac{1}{\sqrt{a_f^2 + b_f^2 + 1}}\right). \tag{7}$$

The validity of θ_f were judged by the probability values of the *F*-statistic, which tests the significance of the regression through an analysis of variance (Zar, 1984). The θ_f for which $p < 0.05$ are considered to be valid estimations of non-zero seabed slope. Those not meeting this criterion were inferred to be approximately zero and were generally from a rough seabed at near-perpendicular incidence. The non-zero seabed slopes are plotted against longitude, latitude, and depth in Figure 5.

Seabed classification

The S_s of the seabed, its variance, spectra, and directivity within the coherent and incoherent seabed scatter provide metrics for hardness and roughness. However, backscatter from the seabed depends on the insonified area, which is a function of the constant ψ, and variable z and θ. As revealed below, metrics for hardness and roughness are deconvolved from these dependences.

Following Manik *et al.* (2006), for normal incidence on a flat seabed, the average surface-scattering coefficient ($\overline{S_s} = 10^{\overline{S_v}/10} \times T$; $\mathrm{m}^2\ \mathrm{m}^{-2}$) is equivalent to the mean area-backscattering coefficient ($\overline{s_a}$; $\mathrm{m}^2\ \mathrm{m}^{-2}$), where T is the thickness (m) of the integration layer. This relationship is only a rough approximation when the seabed is not flat. Here, T is T_i, the thickness of the coherent seabed echo for the ith 25-m long integration-averaging interval. Estimates of the zero-roughness echo amplitude (p_0) and the rms roughness (ρ) are derived from the first moment of the coherent reflection from a rough surface having a Gaussian PDF (Medwin and Clay, 1998):

$$\overline{p_{i,f}} = p_{0_i} \mathrm{e}^{-2k_f^2 \rho_i^2 \cos^2 \overline{\phi_{i,f}}}, \tag{8}$$

where the mean pressure of the seabed echo $\overline{p_{i,f}} = \sqrt{\overline{s_{s_{i,f}}}}$ was estimated from the coherent seabed echo for each i and f, and $\phi_{i,f} = \theta_{i,f}$ for a vertical echosounder. Using $\overline{p_{i,f}}$ and $\overline{\theta_{i,f}}$, Equation (8) was inverted to estimate p_{0_i} and ρ_i using a non-linear, least-squares fit. When $k\rho \cos\theta$ is small, the echo is mostly reflected; as it increases, the coherent echo diminishes exponentially and the incoherent component increases. For large $\theta_{i,f}$, a number of additional considerations are warranted (Medwin and Clay, 1998).

Averaging $\overline{p_{i,f}}$ over all frequencies ($\overline{p_i}$) and dividing by p_{0_i} yields a metric of hardness. Averaging the incoherent portion of the seabed scatter ($\overline{p_{d_{i,f}}} = \sqrt{\overline{s_{s_{i,f}}}}$) over all frequencies ($\overline{p_{d_i}}$) and dividing by p_{0_i} yields a metric of roughness [$20 \log(p_d/p_0)$]. Then T is T_i, the thickness of the incoherent seabed echo. Note that these metrics are independent of the beam geometries, range to the seabed, and seabed slope, except for consideration of the decreasing sample resolution (i.e. increasing insonified area) with depth. The roughness metric was mapped to illustrate the expected associations of high-relief rocky seabed with aggregations of rockfish on the top of the 43 Fathom Bank (Figure 6).

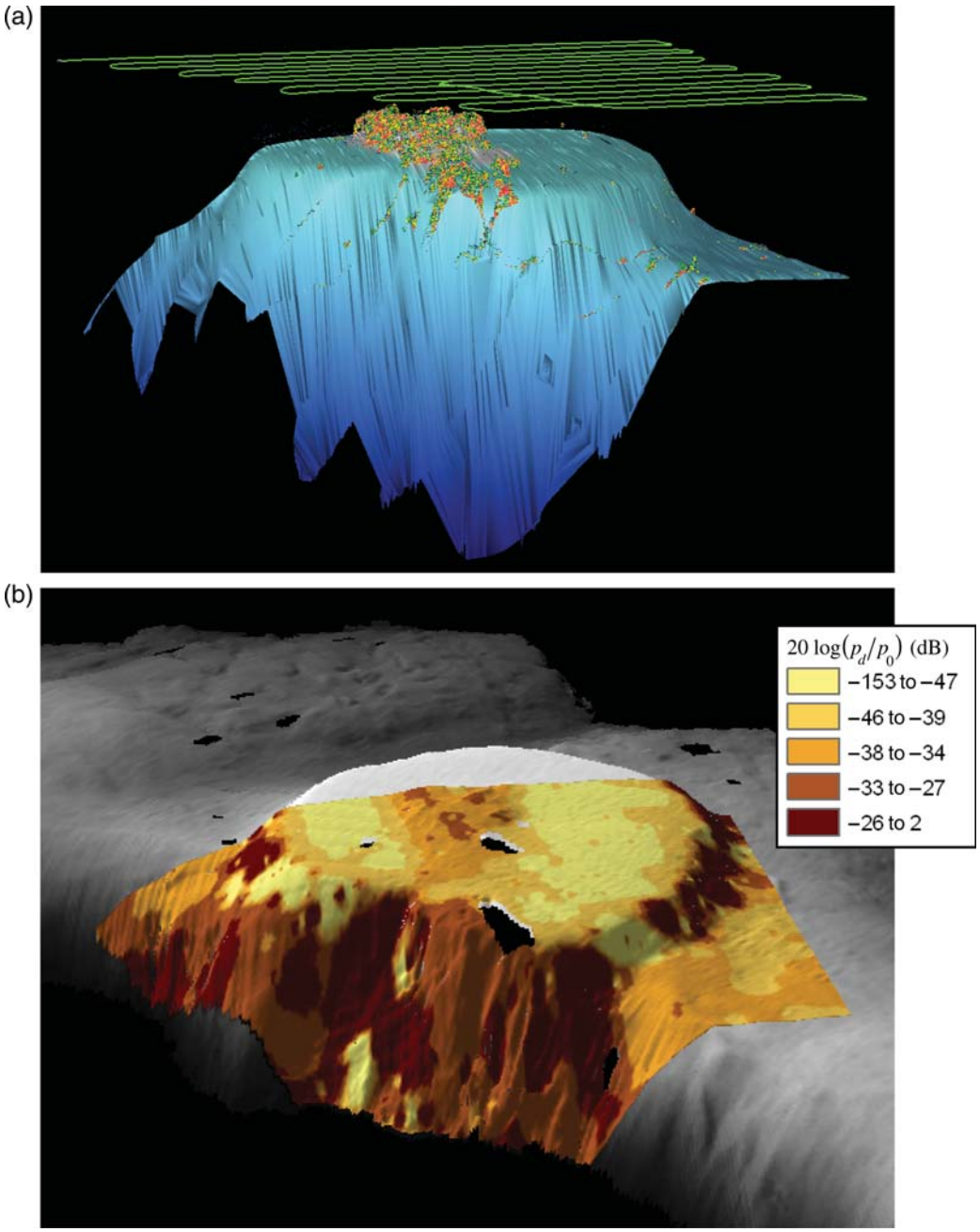

Figure 6. (a) The acoustically sensed distribution of rockfish on the 43 Fathom Bank; (b) a grey-scale image of the seabed bathymetry (courtesy of Chris Goldfinger and Chris Romsos, Oregon State University and Mary Yoklavich, SWFSC) colourized with a roughness metric [20 log(p_d/p_0); dB]. The high-relief rocky areas on the top of the bank are indicated by higher values (darker colours). Voids indicate incomplete bathymetry data.

Classifications of rockfish

During the survey, the s_A attributed to rockfish were mapped in plan view, and the geographical representation (GEOTIFF) was used to navigate the ROV to obtain high-resolution underwater images and information on fish species and sizes. Therefore, the s_A attributed to rockfish was further apportioned to the various species present.

Results

The five-frequency VMR was computed from Equation (4), and distinctly different distributions for the aggregations of rockfish and the coherent seabed were used to identify the echogram pixels as coherent scatter from the seabed, or as relatively incoherent scatter from the seabed and aggregations of rockfish (Figure 2). Therefore, the scatter from demersal fish was separated efficiently and objectively from that of the coherent seabed. The aggregations of rockfish were then mapped and observed with cameras deployed on an ROV. The VMR is also useful to identify other echogram features, such as the transmit pulse, dropouts from bubble attenuation, and scattering from bubbles, plankton, zooplankton, schooling vs. swarming aggregations, and fish without swimbladders.

The z_f, $h_{ADZ,f}$, and θ_f were estimated using Equations (5)–(7) for each transmission and frequency. The $z_{ADZ,f}$, estimated from the range to the initial coherent seabed echo, were smaller than the ranges estimated by the echosounder's amplitude-based, seabed-detection algorithm. In a few instances, $z_{ADZ,f}$ was erroneously estimated as the depth of a resolved single fish. The z_f were consistently larger than the amplitude-based bottom estimates. Throughout the survey, the $h_{ADZ,f}$ ranged from <1 to $\sim$50 m, depending mostly on the transducer beam width, the z_f, and θ_f (see graph of the first 250 pings in Figure 4).

The multifrequency estimates of θ_f appear to be accurate indications of the seabed slope within the insonified (local or within-beam) area. The estimates of local slope are distinctly different for 18 kHz (Figure 5), compared with the higher frequencies (not shown), suggesting biases that could depend on the beam width and frequency. Fine-scale seabed roughness can influence the estimates of local θ_f, especially when the larger-scale seabed slope is low (e.g. flat areas with rocks). This situation causes higher variability and enhanced frequency dependence in the estimates of θ_f.

Estimates of ρ_i at the 43 Fathom Bank are mostly ($>$90%) $<$0.02 m and form a multimodal distribution. Estimates of p_{0_i} are mostly $<$0.8 μPa, and they too are multimodal. The most extreme values of ρ_i and p_{0_i} are generally associated with the steepest edges of the bank and may therefore be inaccurate (Medwin and Clay, 1998).

The three-dimensional map of the roughness metric $[20\log(p_d/p_0)]$ on the 43 Fathom Bank (Figure 6) is in good agreement with visual observations from the ROV. Specifically, the top of the bank includes large areas of high-relief rock and some lower-relief rocky areas with sand. Rockfish are consistently mapped in these rocky areas, particularly amid the high-relief rocks. The steep edges of the bank are mostly scoured rock, and the plains to the southeast, in the lee of the bank, are covered with gravel and sand.

Discussion

In cases when the PDFs of VMR are too broad to distinguish between scatterers of interest, extremal statistics could be employed with multifrequency echosounder data to reduce the size of the temporal-spatial averaging bins by the number of frequencies employed. For example, instead of preclassifying with the VMR as calculated in Equation (4), an extremal-VMR (VMR_{ex}) could be calculated from the peak values of $e_{p,f}$ collected over a depth range and several transmissions (i.e. a temporal-spatial bin). Compared with VMR, the VMR_{ex} has reduced variance, depending on the number of frequencies and their bandwidth. This means that the averaging bin-sizes for multifrequency analyses can be reduced at least by a factor equal to the number of frequencies employed. Additionally, because the PDF of VMR_{ex} is expected to be radically different for resolvable individual vs. overlapping targets (Figure 1b vs. c; see also Stanton and Clay, 1986), VMR_{ex} could be useful for improving single-target detections, and estimating target strengths and critical densities (Trevorrow, 1996).

Both the echo amplitude and phase at multiple-frequencies provide useful information for identifying biological targets and estimating their aggregation densities, abundances, and behaviours, and detecting and classifying the seabed. For example, the variability of signal phase within single-target echoes can indicate the target size and orientation (Barr and Coombs, 2005). For overlapping echoes from fish, MacLennan *et al.* (2004) observed that α and β were highly variable, as expected, and the ping-to-ping variation was essentially random. In this paper, information in the signal phase is demonstrated to improve estimates of seabed depth, slope, hardness, and roughness. Scientific-echosounders should provide sample data so that the combination of echo amplitudes, and intra- and inter-channel phases can be better exploited.

Conclusion

The efficacies of multifrequency and single-frequency statistical techniques are challenged by the usual requirement to group echo measurements to facilitate meaningful comparisons with model predictions. Groupings of data over space, time, or both can combine scatter from multiple taxa or species, or from demersal fish and the seabed, which can confound the comparisons and bias results. This problem is mitigated with the SSID, which uses multifrequency echo statistics (VMR) from individual time-space-records (pixels) to identify general scatterer types before applying model-based identification schemes for taxa- or species-level identifications. It is effective for fine-scale detections and classifications of individual and aggregated fish, and the reflected and scattered components of seabed echoes. It is also useful for the efficient separation of scatter from demersal fish and the seabed and facilitates estimates of local, within-beam seabed slope, hardness and roughness, and the height of the dynamic ADZ, for each transmission and frequency.

Combining accurate measurements of seabed range and local, within-beam slope over a broad bandwidth and range of grazing angles should provide much new information for better acoustic seabed classifications. Broad-bandwidth, multibeam systems with split-beam configurations, e.g. Simrad ME70 and MS70, are poised to exploit these new methods.

Acknowledgements

We appreciate the contributions of Captain Ken Franke (CPFV "Outer Limits"), Deanna Pinkard (SWFSC), and Derek Needham (Sea Technology Services) to the initial COAST surveys of rockfish in the SCB. We also thank Nancy Lo (SWFSC) for discussions related to the PDF resulting from fixed-number samplings of multiple Rician PDFs.

References

Barr, R., and Coombs, R. F. 2005. Target phase: an extra dimension for fish and plankton target identification. Journal of the Acoustical Society of America, 118(3 Part 1): 1358–1371.

Carlson, T. J., and Jackson, D. R. 1980. Empirical evaluation of the feasibility of split beam methods for direct *in situ* target strength measurement of single fish. Seattle Applied Physics Laboratory, University of Washington. 43 pp.

Clay, C. 1983. Deconvolution of the fish scattering PDF from the echo PDF for a single transducer sonar. Journal of the Acoustical Society of America, 73: 1989–1994.

Clay, C. S., and Heist, B. 1984. Acoustic scattering by fish: acoustic models and a two parameter fit. Journal of the Acoustical Society of America, 75: 1077–1083.

Conti, S. G., Demer, D. A., Soule, M. A., and Conti, J. H. E. 2005. An improved multiple-frequency method for measuring *in-situ* target strengths. ICES Journal of Marine Science, 62: 1636–1646.

Dahl, P., and Mathisen, O. 1983. Measurement of fish target-strength and associated directivity at high frequency. Journal of the Acoustical Society of America, 73: 1205–1211.

Demer, D. A. 2004. An estimate of error for the CCAMLR 2000 survey estimate of krill biomass. Deep Sea Research II, 51: 1237–1251.

Demer, D. A., and Conti, S. G. 2003. Reconciling theoretical versus empirical target strengths of krill; effects of phase variability on the distorted-wave Born approximation. ICES Journal of Marine Science, 60: 429–434. Erratum 2004, 61: 157–158.

Demer, D. A., Soule, M. A., and Hewitt, R. P. 1999. A multifrequency method for improved accuracy and precision of *in-situ* target strength measurements. Journal of the Acoustical Society of America, 105: 2359–2376.

Foote, K. G. 1983. Linearity of fisheries acoustics, with addition theorems. Journal of the Acoustical Society of America, 73: 1932–1940.

Greenlaw, C. F. 1979. Acoustical estimation of zooplankton populations. Limnology and Oceanography, 24: 226–242.

Greenlaw, C. F., and Johnson, R. K. 1983. Multiple-frequency acoustical estimation. Biological Oceanography, 2: 227–252.

Hewitt, R. P., Watkins, J. L., Naganobu, M., Tshernyshkov, P., Brierley, A. S., Demer, D. A., Kasatkina, S., *et al.* 2002. Setting a precautionary catch limit for Antarctic krill. Oceanography, 15: 26–33.

Holliday, D. V., and Pieper, R. 1980. Volume scattering strengths and zooplankton distributions at acoustic frequencies between 0.5 and 3 MHz. Journal of the Acoustical Society of America, 67: 135–146.

Holliday, D. V., Pieper, R. E., and Kleppel, G. S. 1989. Determination of zooplankton size and distribution with multifrequency acoustic technology. Journal du Conseil International pour l'Exploration de la Mer, 46: 52–61.

Korneliussen, R. J., and Ona, E. 2002. An operational system for processing and visualizing multi-frequency acoustic data. ICES Journal of Marine Science, 59: 293–313.

MacLennan, D. N., Copland, P. J., Armstrong, E., and Simmonds, E. J. 2004. Experiments on the discrimination of fish and seabed echoes. ICES Journal of Marine Science, 61: 201–210.

Manik, H. M., Furusawa, M., and Amakasu, K. 2006. Quantifying sea bottom surface backscattering strength and identifying bottom fish habitat by quantitative echo sounder. Japanese Journal of Applied Physics, 45: 4865–4867.

Medwin, H., and Clay, C. S. 1998. Fundamentals of Acoustical Oceanography. Academic Press, Boston, MA. 712 pp.

Ona, E., and Mitson, R. B. 1996. Acoustic sampling and signal processing near the seabed: the dead zone revisited. ICES Journal of Marine Science, 53: 677–690.

Peterson, M., Clay, C., and Brandt, S. 1976. Acoustic estimates of fish density and scattering function. Journal of the Acoustical Society of America, 60: 618–622.

Shirazi, M. A., de Moustier, C., Cervenka, P., and Zisk, S. H. 1992. Differential phase estimation with the SeaMARC II bathymetric sidescan sonar system. IEEE Journal of Oceanic Engineering, 17: 239–251.

Stanton, T. K., and Clay, C. S. 1986. Sonar echo statistics as a remote-sensing tool: volume and seafloor. IEEE Journal of Oceanic Engineering, 11: 79–95.

Tesler, W. D. 1989. Bias and precision in acoustic biomass estimation. Proceedings of the Institute of Acoustics, 11: 202–211.

Trevorrow, M. V. 1996. Multifrequency acoustic investigations of juvenile and adult fish in Lake Biwa, Japan. Journal of the Acoustical Society of America, 100: 3042–3052.

Zar, J. H. 1984. Biostatistical Analysis. Prentice-Hall, Inc., Englewood Cliffs, NJ, USA. 718 pp.

doi:10.1093/icesjms/fsp054